forum acusticum 2026
8-12 September · Graz, Austria

Analytical Investigation of Sound Diffraction by Straight and Serrated Trailing Edges

Nafsika Papantonopoulou[1], Penelope Menounou[1], Petros Nikolaou[1]

[1]*Department of Mechanical Engineering and Aeronautics, University of Patras, Greece*

Abstract

This work investigates sound diffraction around an airfoil trailing edge, modeled as a half-plane, using a newly presented Green's function for infinite and finite diffracting edges. It is shown that when a point source is on or near the wing surface, the diffracted field can dominate the total sound field. An equation to estimate this importance in advance is provided. The model is then extended to serrated trailing edges and comparisons are provided against straight trailing edges. Tests across different receiver planes and source locations show that serrations can reduce noise for some receivers but increase it for others, so the best design depends on the source-receiver configuration. However, serrations with segment length of wavelengths and inclination angle perform reasonably well in most cases. The greatest noise-reduction benefit appears underneath the wing, except when the source is exactly at the trailing edge, in which case the serration does provides marginal benefit or even marginal disadvantage by increasing the noise field.

Keywords: *diffraction, analytical solution, serrated trailing edge, jet noise shielding*

1. Introduction

In aeroacoustic applications, we often study how extended surfaces affect the radiated sound field. Examples include the effect of an aircraft wing on engine noise, trailing-edge noise, and sound generated by a deployed flap and diffracted by the main wing. Surfaces may participate in noise generation through interactions with the flow (active surfaces) or redirect sound through scattering/reflection and diffraction (passive surfaces). These phenomena have been studied analytically, numerically, and experimentally, and considerable effort has gone into reducing noise by replacing straight trailing edges with serrated ones (see, for example, Ref. [1]).

In many analytical studies, sound generation and sound propagation are combined in a single model, often valid

replacing straight trailing edges with serrated ones (see, for example, Ref. [1]).
In many analytical studies, sound generation and sound propagation are combined in a single model, often valid

only in the far field. This makes it difficult to determine whether discrepancies between predictions and experiments arise from the source model or from the propagation model. One class of analytical approaches uses tailored Green's functions. Howe[2] developed one of the earliest analytical models for serrated trailing edges, and later studies suggested that discrepancies with measurements were likely due to inaccuracies in the Green's function. More recently, Lyu[3] presented a tailored Green's function, which is nevertheless restricted to high frequencies.

In the present work, we focus on the propagation problem and treat the wing as a passive surface. We employ a newly presented Green's function[4], valid for all source and receiver locations, all frequencies, and for both infinite- and finite-length diffracting edges, to construct diffraction models for straight and serrated trailing edges. Earlier work by the authors[5] showed that certain serration profiles can improve shielding relative to a straight edge, but only for receivers in the shadow zone and for sources several wavelengths away from the edge. Here, we consider source locations more representative of aeroacoustic applications, including sources near the wing surface and trailing edge, as well as low and high frequencies. Finally, we examine receivers on multiple planes around the edge, not just in the shadow zone.

2. Theory/ Mathematical Formulation

2.1 Diffraction by an infinitely long edge

The present work employs a newly derived Green's function solution[4] for the canonical problem of sound diffraction by a rigid half plane (Fig. 1). The half-plane represents the wing and its trailing edge in its simplest form. The sound source is placed at locations representative of typical aeroacoustics problems (on the surface of the wing, at the trailing edge, or at the exhaust of an engine close to the trailing edge). The presence of the wing changes the acoustic field produced by the sound source. The wing causes sound (i) to reflect on the wing surface, and (ii) to diffract around the trailing edge.

Corresponding author: up1072425@ac.upatras.gr.

The total acoustic field is composed of diffraction contributions (P_{diff}) and geometrical acoustics contributions (P_{inc}, P_{ref}),

$$P_{total} = P_{inc} + P_{ref} + P_{diff} \,, \tag{1}$$

where P_{inc} is the field coming from the source, P_{ref} is the field coming from the image-source, and P_{diff} is the diffracted field.

The geometrical acoustics contribution for a spherical wave is

$$P_{inc} = \frac{e^{ikR_{inc}}}{R_{inc}}, P_{ref} = \frac{e^{ikR_{ref}}}{R_{ref}} \,, \tag{2}$$

where $k = 2\pi f / c_0$ is the wavenumber, f is the frequency, c_0 is the speed of sound, R_{inc} is the direct distance between the source and the receiver, and R_{ref} is the direct distance from the image-source to the receiver (see Fig. 1)

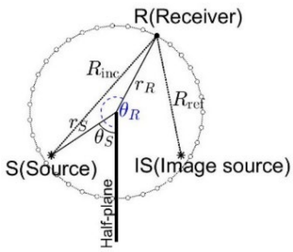

Figure 1. Geometry of the half plane diffraction problem; side view.

The newly presented Green's function proposes the following analytical solution for the diffracted field,

$$\begin{aligned} P_{diff} &= -\int_0^1 P_{inc}\left(L_z\left(Y_z\right)\right) dM \\ L_z\left(Y_z\right) &= \sqrt{2 r_S r_R \left(\cosh\left(4 \arctan h\left(Y_z\right)\right) - 1\right) + L^2} \end{aligned} \,, \tag{3}$$

where L_z is the reradiation path from the source to a point z on the edge and then to the receiver (see Fig. 2), M is given as

$$\begin{aligned} M &= M_{++} + M_{+-} + M_{-+} + M_{--} \\ M_{\pm\pm} &= \frac{1}{\pi} sign\left(\sin\left(b_{\pm\pm}\right)\right) \arctan\left[d_{\pm\pm} Y_z\right], \\ d_{\pm\pm} &= \sqrt{\frac{1+\cos\left(b_{\pm\pm}\right)}{1-\cos\left(b_{\pm\pm}\right)}}, b_{\pm\pm} = \frac{\pi \pm \theta_R \pm \theta_S}{2} \end{aligned} \tag{4}$$

while Y_z is a normalized edge length that varies from 0 (corresponds to the shortest reradiation path, L) to 1 (corresponds to the reradiation path going through the edge point at infinity).

2.2 Diffraction by a finite-length edge

For diffraction by a finite edge, the solution for an infinitely long segment is employed [Eq.(4)] but with the diffraction field given as the sum of two integrals

$$\begin{aligned} P_{diff} &= \pm I_1 + I_2 \\ I_{1,2} &= \frac{1}{2}\int_0^{Y_{1,2}} P_{inc}\left(L_z\left(Y_z\right)\right) dM \end{aligned} \tag{5}$$

where, $Y_{1,2}(L_{1,2})$ is the normalized edge length that corresponds to the end of the segments z_1 and z_2 with re-radiation paths L_1 and L_2, respectively (as shown in Fig. 2). The $+$ sign in front of I_1 in Eq.(5) corresponds to the configuration in Fig. 2a) and the $-$ sign to the configuration in Fig. 2b).

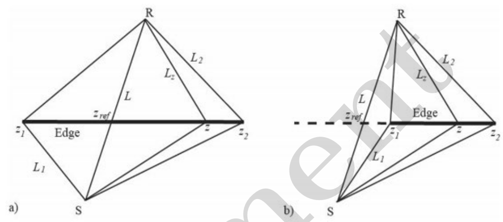

Figure 2. Diffraction by a finite edge length; a) when the shortest reradiation path, L, intersects the edge, b)when the shortest reradiation path, L, does not intersect the edge.

2.3 Diffraction by a serrated edge

The serrated edge geometry is modeled as a sequence of finite-length teeth (as shown in Fig. 3), where each tooth consists of two segments with length L expressed as a multiple of the wavelength λ, and inclination angle α. Each segment is treated as a finite diffracting edge and a local cartesian coordinate system aligned with the segment is employed.

For a serrated edge composed of N teeth, the total diffracted field is written as the superposition of the diffracted contributions from all finite segments,

$$P_{diff}^{serrated} = \sum_{m=1}^{N} \sum_{s=1}^{2} P_{diff}^{(m,s)} \tag{6}$$

where m denotes the tooth index and s denotes either the upper $(s = 1)$ or the lower segment $(s = 2)$ of each tooth. For each segment, the source and receiver coordinates in the global cartesian coordinate system ((x_S, y_S, z_S) and (x_R, y_R, z_R), respectively) are first translated to a local cartesian system at the segment midpoint $(x_M, y_M, z_M)^{(m,s)}$

$$\begin{aligned} (x_S, y_S, z_S)^t &= (x_S, y_S, z_S) - (x_M, y_M, z_M)^{(m,s)}, \\ (x_R, y_R, z_R)^t &= (x_R, y_R, z_R) - (x_M, y_M, z_M)^{(m,s)} \end{aligned} \tag{7}$$

The translated source $(x_S, y_S, z_S)^t$ and receiver $(x_R, y_R, z_R)^t$ positions are then expressed in a rotated local coordinate system aligned with the segment. The rotation angle is $\varphi = (-1)^s a$. For each segment, the transformation is

$$\begin{aligned} x' &= x^t \cos\varphi + z^t \sin\varphi, \\ z' &= -x^t \sin\varphi + z^t \cos\varphi, \\ y' &= y^t. \end{aligned} \tag{8}$$

The transformation in Eq. (8) is applied to both the source and receiver coordinates. The transformed cartesian coordinates are then converted to cylindrical coordinates, and the finite-edge diffraction [Eq.(5)] is evaluated. The total diffracted field is obtained by summing the contribution of all inclined finite-edge segments.
For the geometrical acoustics contribution, the incident and reflected fields are added to compute the total acoustic field. The incident field is included only if the source is visible through all serration teeth. In other words, if any tooth blocks the direct source-receiver path, the incident contribution is not included in the solution. In contrast, the reflected field is included, if it reaches the receiver through reflection by at least one tooth. Many repeated teeth are used in the spanwise direction so that the ends of the serration profile do not affect the results in the middle of the profile. Higher order diffraction effects between neighboring segments are neglected.

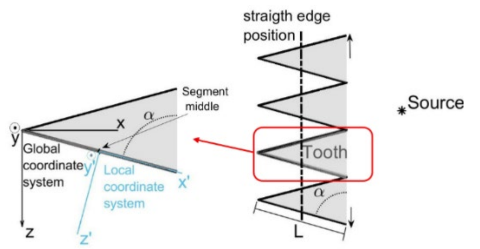

Figure 3. Serrated edge profile geometry.

3. Diffraction around straight edges

In this section, we investigate the contribution of diffraction to the total acoustic field in cases where the sound source is positioned at locations relevant to aeroacoustic problems (i.e. close to the trailing edge and/or close to the wing surface).
For the numerical evaluation, we consider sound sources of different frequencies varying from $5Hz$ to $2500Hz$, different radial distances from the edge, r_S, varying from $0.0001m$ to $0.1m$, and different angular locations, θ_S, varying from 0° (on the surface of the wing) to 180°. For all combinations of source location and frequency we compute the acoustic field at receivers located at a circular array around the edge (see Fig. 1) with the angular location of each receiver, θ_R, varying from 0 to 2π. The computations are repeated for different radial distances of the receivers, r_R, varying from $2m$ to $10m$.
To quantify the relative contribution of diffraction to the total acoustic field, the following ratio is evaluated over all receiver locations θ_R around the edge of the half-plane:

$$D = \frac{\int_0^{2\pi} \left|P_{diff}(\theta_R)\right|^2 d\theta}{\int_0^{2\pi} \left|P_{total}(\theta_R)\right|^2 d\theta}. \quad (9)$$

Values of D close to unity indicate that the acoustic field is dominated by diffraction effects, whereas smaller values imply a weak diffraction contribution to the total sound field.
The numerical investigation revealed that D is influenced primarily by the normalized radial distance of the source from the trailing edge, kr_S, and of the angular location of the source w.r.t the surface of the wing θ_S. Figure 4 shows results for two receiver radii r_R. It can be observed that diffraction becomes a dominant contribution as the source approaches the edge $(kr_S \to 0)$ and as the source moves closer to the wing surface $(\theta_S \to 0)$. On the other hand, for $kr_S > 1$ the diffraction contribution decreases substantially, indicating that diffraction becomes weak when the source is sufficiently far from the edge.
To better define the transition between diffraction-dominated and non-diffraction-dominated regions, we provide the following fitted curves for $D = 0.15$, $D = 0.60$ and $D = 0.85$ respectively:

$$kr_S = \begin{cases} 1.301\theta_S^2 - 1.258\theta_S + 1.066, 0 <= \theta_S <= 0.4 \\ -2.609\theta_S^2 + 2.578\theta_S + 3.054, 0.4 < \theta_S <= 1.3 \\ -1.511\theta_S^3 + 8.4\theta_S^2 - 15.697\theta_S + 10.6, 1.3 < \theta_S <= 2.65 \end{cases}, (10)$$

$$\theta_S = -5.01 kr_S^{(0.5635)} + 1.26 \quad (11)$$

$$\theta_S = -3.319 kr_S^{(0.3811)} + 0.57 \quad (12)$$

These fitted curves provide a practical a priori criterion for estimating whether diffraction is negligible, important, or dominant based only on frequency and source position relative to the wing. It is noted that all fitted curves show only minor deviations between different receiver radii.

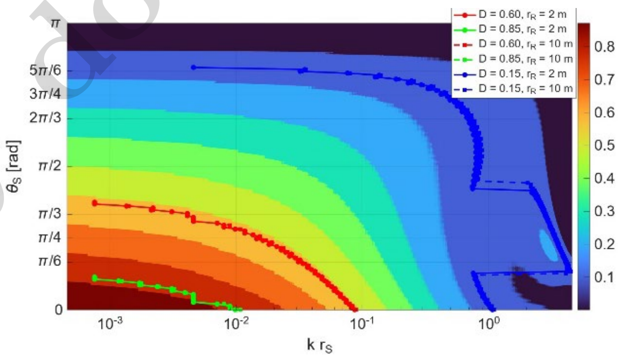

Figure 4. Contours of the diffraction contribution parameter D for different θ_S and kr_S values. Solid lines correspond to $r_R = 2m$, dashed lines correspond to $r_R = 10m$

4. Performance of Serrated Edges

The question that we address in this section is whether a serrated edge can reduce the noise field compared to a straight edge.

4.1 Serrated edge profiles

Multiple serration profiles are investigated by varying the two geometrical parameters of the serration, i.e. the normalized segment length L/λ and the inclination angle α. Each serrated profile is compared against the corresponding straight edge profile that passes through the midpoint of the serration segments (see Fig. 3).

4.2 Control receiver planes

The receivers are placed on xy and xz planes (see Fig. 5). The xz receiver planes are planes parallel to the wing surface at both positive and negative y positions: xz planes with positive y positions are on the source side and are denoted as xz_+, while xz planes with negative y positions are denoted as xz_-. The xy receiver planes are perpendicular to the wing surface at z positions passing through the middle point of a serration tooth and they are denoted xy_m. Finally, with $xz_{-,uw}$ we denote only the receivers on a xz_- plane that are underneath the wing($y_R < 0$ and $x_R > 0$). Similarly, with $xy_{m,uw}$ we denote only receivers on a xy_m plane that are underneath the wing. In both these cases, the receivers are in the shadow zone provided by the wing surface.

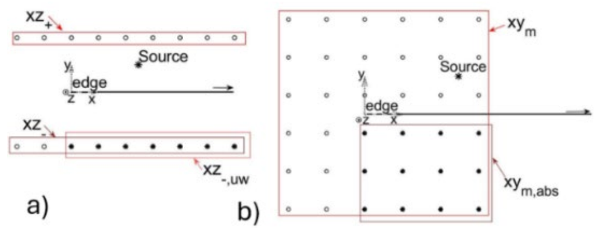

Figure 5. Receivers control planes: a) xz_+, xz_- and $xz_{-,uw}$ planes, $y = \pm 5$ b) xy_m, $xy_{m,uw}$ planes, z closest possible to z_S.

4.3 Measure of performance

The acoustic performance of each serration profile is compared to the corresponding straight edge profile as follows:

$$\Delta SPL(R) = SPL_{straight}(R) - SPL_{serrated}(R), \quad (13)$$

where $SPL_{straight}(R)$ is the SPL at receiver R when the trailing edge is a straight line and $SPL_{serrated}(R)$ is the SPL at the same receiver when the trailing edge is serrated. Positive values of $\Delta SPL(R)$ indicate that the trailing edge reduces the noise field at R (a positive performance), while negative values indicate an increase in the sound level and thus a negative performance of the serrated profile.

For each serration profile tested, in other words for each pair of geometrical parameters $(a, L/\lambda)$, $\Delta SPL(R)$ is computed for each receiver on a specific receiver control plane. Then, the arithmetic mean value over all receiver locations on that receiver control plane, $\overline{\Delta SPL}$, is evaluated. A positive value of $\overline{\Delta SPL}$ on the receiver plane indicates a positive performance of the serrated profile for the entire control plane. We associate the $\overline{\Delta SPL}$ with the geometrical parameters $(a, L/\lambda)$ of the serration profile that created it and we repeat the process for many serration profiles.

For each one of the control receiver planes, a contour of a and L/λ depicting $\overline{\Delta SPL}$ is created. The pair of a and L/λ that performs the best at each case is determined.

4.4 Location of model sources

We consider the following characteristic source locations: (i) source away from the trailing edge of the wing and away from the surface of the wing (the source was placed at $x_S = 10m$, $y_S = 10m$ which corresponds to approximately 20 wavelengths away from the trailing edge), (ii) source away from the trailing edge but on the surface of the wing (source was placed at $x_S = 10m$, $y_S = 0.0001m$), (iii) source at the trailing edge, specifically the source was placed in the middle of the tooth of a serration. As the corresponding straight edge passes through the middle of the serration teeth, the selected source location is placed on the edge of both the serrated profile and the straight profile, (iv) source placed at $x_S = 3m$, $y_S = 1m$ to approximate the location of the engine exhaust. The frequency is set at $500Hz$ for all cases. Note that source is placed above the wing in all cases, so receivers underneath the wing are in the shadow zone.

4.5 Proposed serration profile

In the following, in Fig. 6-Fig.9 we present the overall performance $\overline{\Delta SPL}$ of the various profiles (combinations of a and L/λ) at the control receiver planes: xz_+, xz_-, $xz_{-,uw}$ (all parallel to the wing of the surface) and xy_m, $xy_{m,uw}$ (both perpendicular to the wing) as described in Section 4.2.

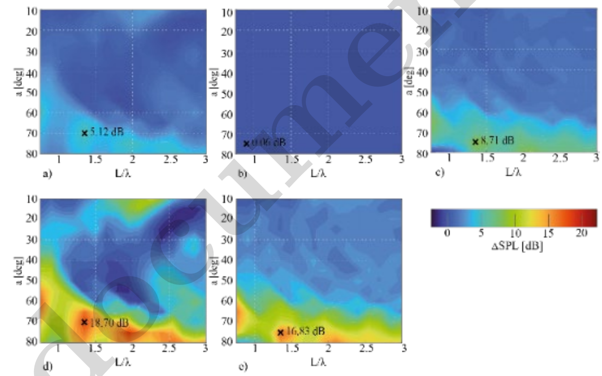

Figure 6. $\overline{\Delta SPL}$ for different a and L/λ values on the various control receiver planes. Source away from the trailing edge and the surface of the wing. Control receiver planes: a) xy_m plane b) xz_+ plane c) xz_- plane d) $xy_{m,uw}$ plane and e) $xz_{-,uw}$ plane. The $\langle\times\rangle$ mark annotates the $(a, L/\lambda)$ pair for optimum performance at each control receiver plane.

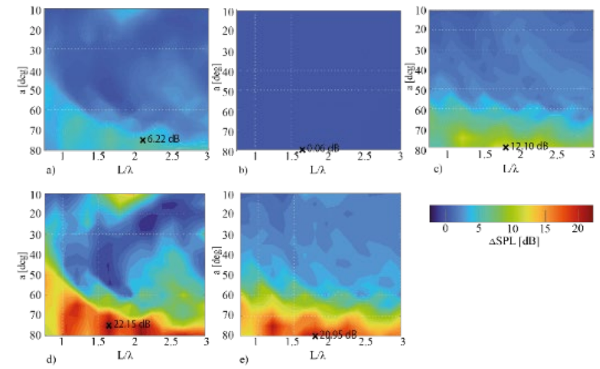

Figure 7. $\overline{\Delta SPL}$ for different a and L/λ values on the various control receiver planes. Source away from the trailing edge and on the surface of the wing. Control receiver planes as described in Fig. 6.

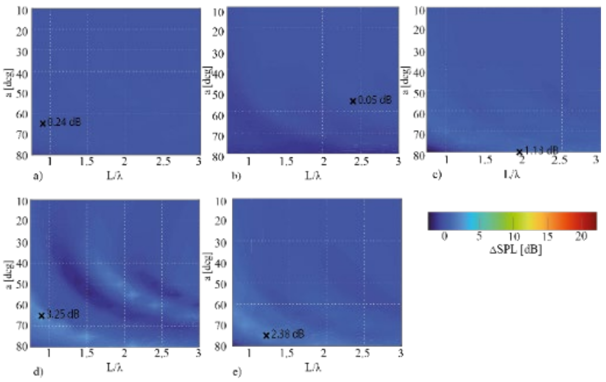

Figure 8. $\overline{\Delta SPL}$ for different a and L/λ values on the various control receiver planes. Source on the trailing edge. Control receiver planes as described in Fig. 6.

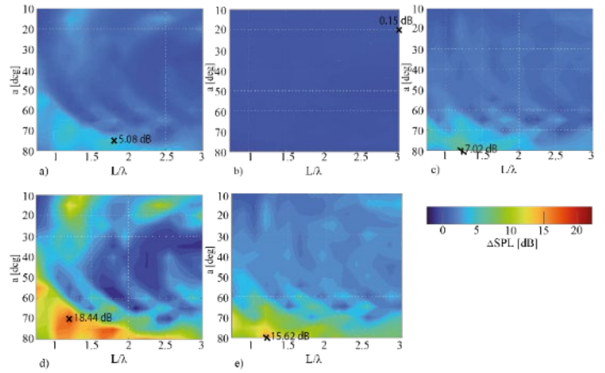

Figure 9. $\overline{\Delta SPL}$ for different a and L/λ values on the various control receiver planes. Source is located at the exhaust of an engine. Control receiver planes as described in Fig. 6.

The following observations can be made:

(i) There is not a single serration design that is optimum for all model source locations and all receiver planes. A serration profile that on average offers increased noise protection at a certain receiver plane does not necessarily offer noise protection at another receiver plane. Similarly, a serration profile that offers increased protection for one source location does not offer the same protection for all source locations. The proposed edge profile has been chosen so that it works well in most cases.

(ii) The shielding effect of the serrated profile is pronounced for receivers located underneath the wing (compare the subplots in the lower row of Fig.6 - Fig.9 compared to the subplots in the upper row)

(iii) Many serration profile designs offer increased noise protection when the source is away from the trailing edge and either on the surface of the wing (see Fig. 7) or away from the surface (see Fig. 6). Less serration profiles offer increased noise protection when the source is at the exhaust of the engine.

(iv) When the source is at the trailing edge, there is a limited number of serration design profiles that offer increased noise protection compared to the straight edge. And even such profiles have limited shielding effect (see Fig. 8).

The serration profile proposed in the present work is one with inclination angle $a = 75^o$ and segment length $L = 1.5\lambda$.

4.6 Performance of proposed serration profile

The serration profile proposed in the present work is not a profile that works for all source and receiver locations. It is simply the one that works reasonably well in most cases. In the following, we showcase its performance for the four characteristic source locations. The following can be observed:

(i) At receiver locations underneath the wing (see areas within the red frames in Fig. 10 – Fig. 13), the serration increases the shielding effect compared to the straight edge in all cases, except when the source is located exactly on the edge (Fig. 12). Also, when the source is located at the exhaust of the engine, the serration increases (instead of decreasing) the noise field close to the edge underneath the wing(see Fig. 13). Finally, when the source is located on the trailing edge (see Fig. 12), the serration increases the noise field in many locations underneath the wing. For noise mechanism where the source is modeled to be close to the edge, the serration does not offer a clear advantage.

(ii) In the illuminated receiver areas (outside the red frames), interference patterns with scales similar to the segment length can be observed. This indicates that serrated and straight trailing edge profiles interchange which one performs better (see Fig. 10, 11 and 13).

(iii) When the source is located on the trailing edge, receiver locations that may benefit by the serration profile, benefit much less than in cases where the source is not located on the edge.

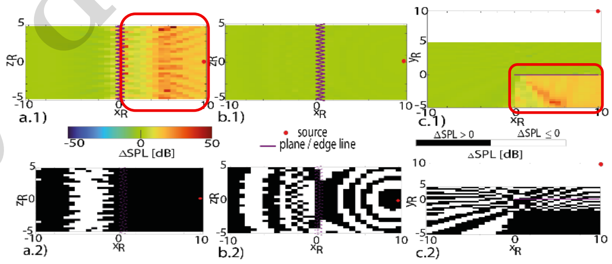

Figure 10. Performance of the proposed serration profile (ΔSPL) and sign of (ΔSPL) for source located away from the trailing edge and away from the wing surface; Control receiver planes: a.1) and a.2): xz_- plane, b.1) and b.2): xz_+ plane, c.1) and c.2): xy_m plane.

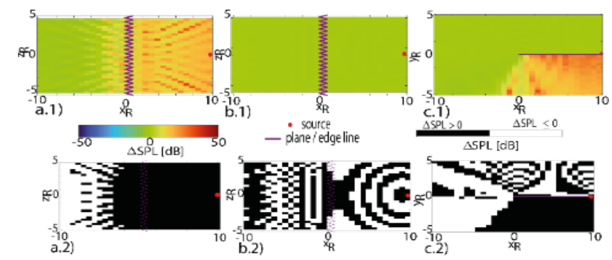

Figure 11. Performance of the proposed serration profile (ΔSPL) and sign of (ΔSPL) for source located on the surface of the wing away from the trailing edge; receiver planes as described in Fig. 10.

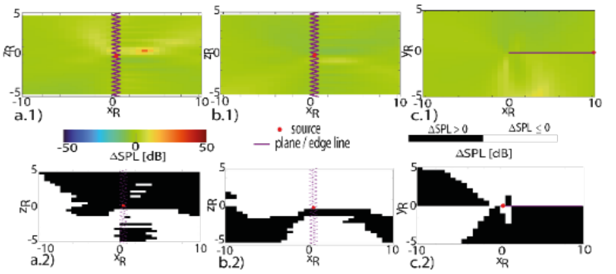

Figure 12. Performance of the proposed serration profile (ΔSPL) and sign of (ΔSPL) for source located on the trailing edge; receiver planes as described in Fig. 10.

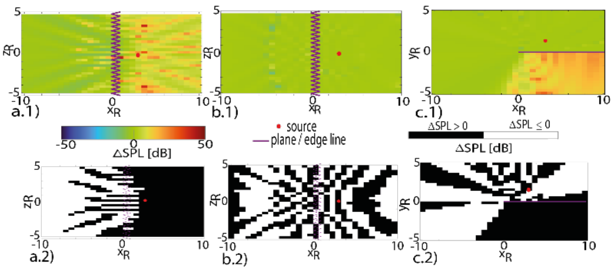

Figure 13. Performance of the proposed serration profile (ΔSPL) and sign of (ΔSPL) for source located at the exhaust of an engine; receiver planes as described in Fig. 10.

5. Conclusions

The present work investigated sound diffraction by straight and serrated trailing edges using a newly presented Green's function for infinite and finite-length diffracting edges, which is valid for all source and receiver locations and all frequencies.

For the straight-edge case it was found that diffraction dominates the total acoustic field when the source is close to the edge (measured in wavelengths) and close to the wing surface. An equation that provides an a-priori estimate of the diffraction contribution to the total field has been provided.

The contribution of serrated edges was obtained by decomposing the serrated profile into multiple inclined finite-length edge segments and adding their individual diffracted contributions. Various serration profiles have been tested for four characteristic source locations and at several control receiver planes. The results demonstrated that serrated trailing edges do not produce uniform attenuation over all receiver positions and for all source locations. A serration profile was proposed that seems to reduce the sound field compared to a traditional straight edge in most cases. The proposed serration profile is one with inclination angle $a = 75^o$ and segment length $L = 1.5\lambda$.

In general, it was shown that for a source located above the wing the proposed serration profile outperforms the straight edge profile at receivers located underneath the wing, except when the source is located exactly on the trailing edge. In the illuminated regions the serrated profile can either increase or decrease the noise field compared to the straight edge. Mitigation of noise mechanisms where the source is modeled as being located on the trailing edge cannot be achieved via serration profiles. Any mitigation observed in related studies of trailing edge noise should be attributed to mechanisms other than diffraction by a serrated edge.

6. Acknowledgments

The present work was financially supported by the «Andreas Mentzelopoulos Foundation».

This paper has been financed by the funding program "MEDICUS", of the University of Patras.

References

[1] S. Lee, L. Ayton, F. Bertagnolio, S. Moreau, T. P. Chong, and P. Joseph, "Turbulent boundary layer trailing-edge noise: Theory, computation, experiment, and application," *Progress in Aerospace Sciences*, vol. 126, 100737, 2021.

[2] M. S. Howe, "Aerodynamic noise of a serrated trailing edge," *Journal of Fluids and Structures*, vol. 5, pp. 33–45, 1991.

[3] B. Lyu, "Analytical Green's function for the acoustic scattering by a flat plate with a serrated edge," *Journal of Fluid Mechanics*, vol. 961, A33, 2023.

[4] P. Nikolaou and P. Menounou, "New Formulation of the exact Green's Function for the Diffraction Field around a Rigid Wedge for efficient Calculations," *in Forum Acusticum 2026* (Graz Austria) accepted abstract.

[5] P. Menounou and J. H. You, "Design of a jagged-edge barrier: Numerical and experimental study," *Noise Control Engineering Journal*, vol. 52, no. 5, pp. 210–224, 2004.